

Supporting Information

Amorphous/amorphous Ni-P/Ni(OH)₂ Heterostructure Nanotubes for Efficient Alkaline Hydrogen Evolution Reaction

Fuzhen Zhao^a, Huicong Liu^a, Houyu Zhu,^b Xiaoyu Jiang^{c,*}, Liqun Zhu^a, Weiping Li^a, Haining Chen^{a,*}

^a School of Materials Science and Engineering, Beihang University, No. 37 Xueyuan Road, Haidian District, Beijing 100191, China

^bSchool of Materials Science and Engineering, China University of Petroleum (East China), Qingdao, Shandong 266580, P. R. China

^c Department of Information Communication, Army Academy of Armored Forces, Beijing 100072, China



Figure S1. Schematic illustration of the axial screw dislocation-driven growth mechanism of Zn@Ni-P NWs.

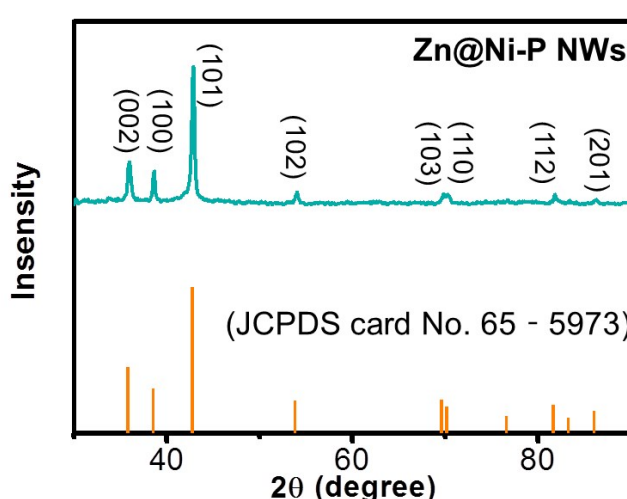


Figure S2. XRD pattern of Zn@Ni-P NWs and the JCPDS card of Zn.

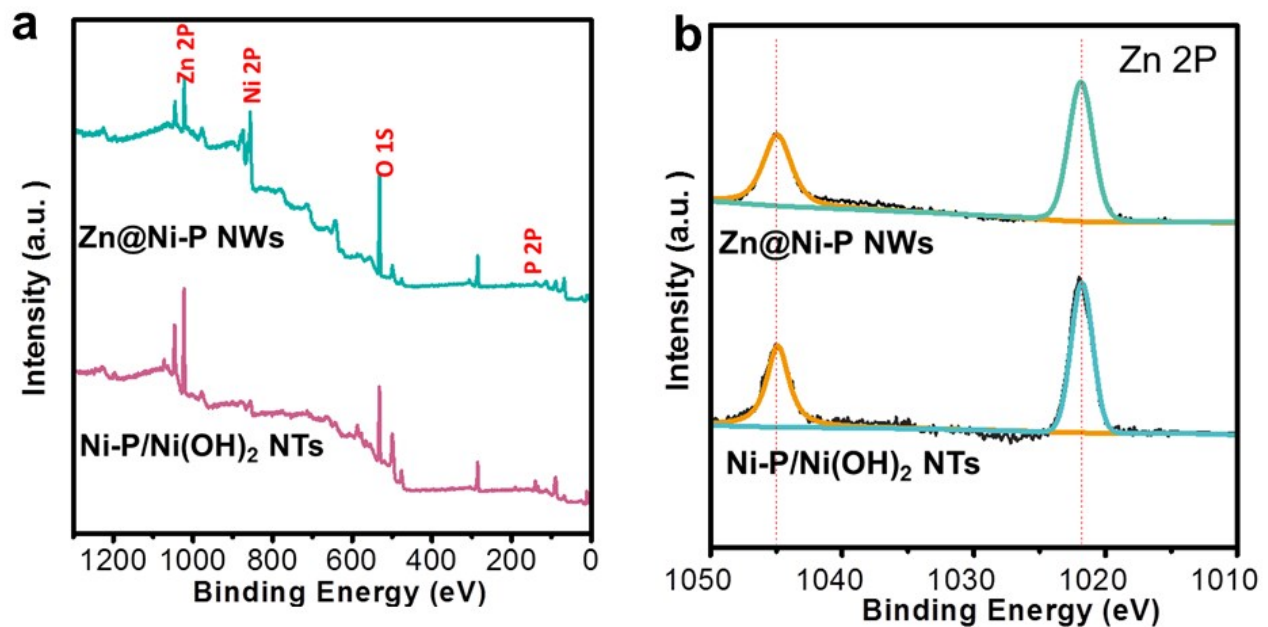


Figure S3. XPS characterization comparison for peaks shift. (a) survey spectra, (b) Zn 2P spectra.

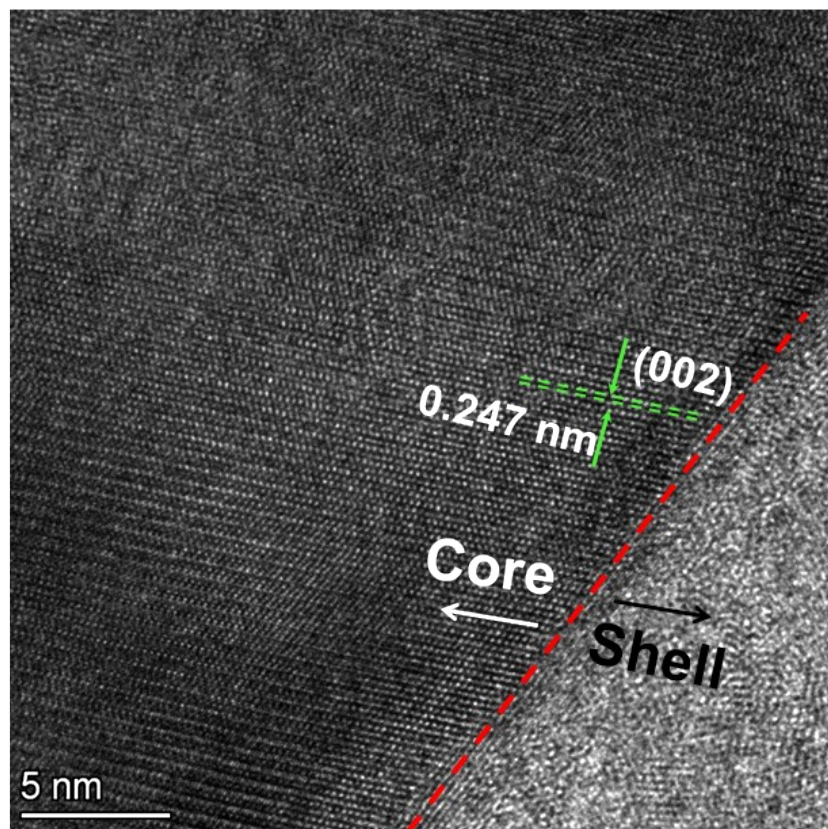


Figure S4. HRTEM image of a core-shell Zn@Ni-P NW.

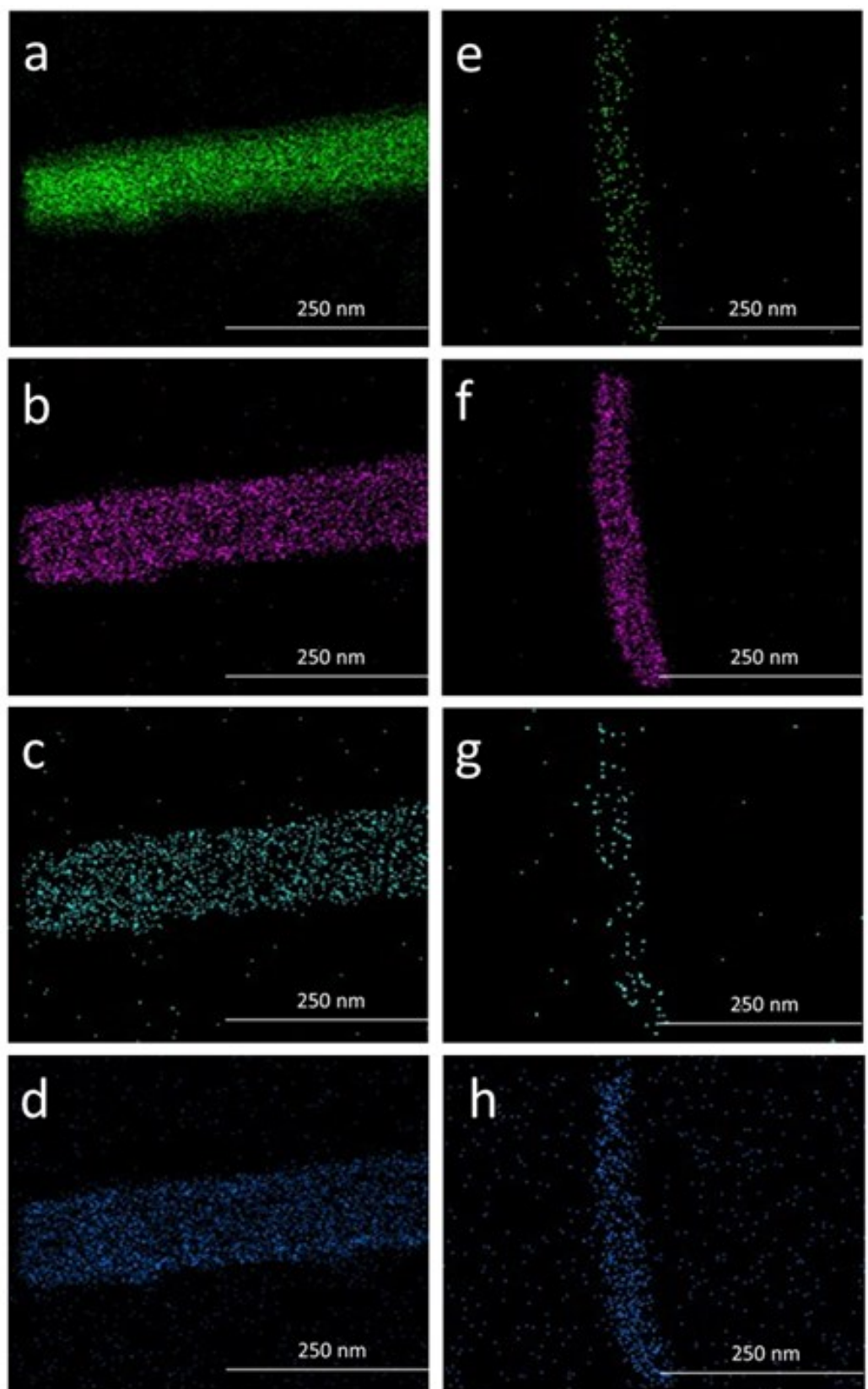


Figure S5. EDS elemental mapping images for Zn (a, e), Ni (b, f), P (c, g) and O (d, h) of Zn@Ni-P NWs (a, b, c and d) and Ni-P/Ni(OH)₂ NTs (e, f, g and h).

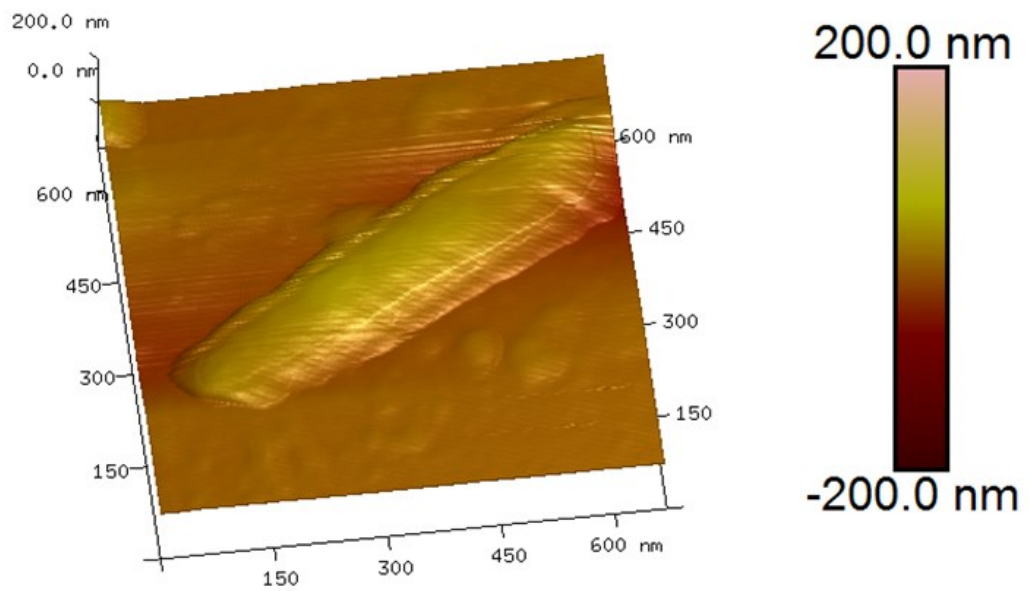


Figure S6. AFM image of a Zn@Ni-P NW.

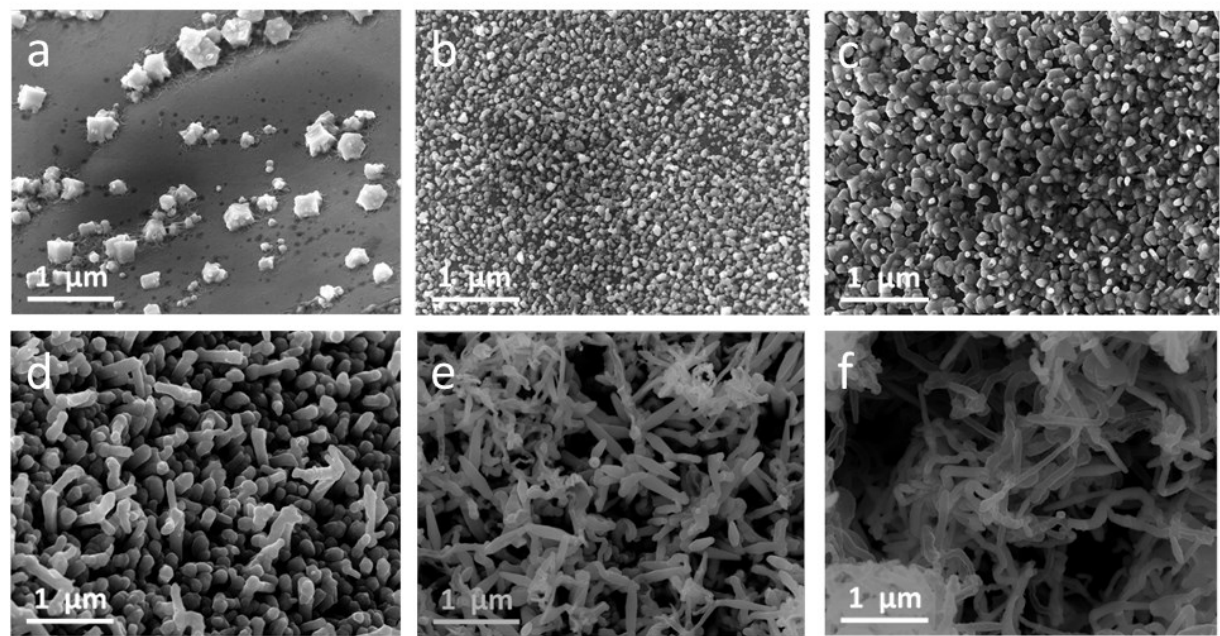


Figure S7. SEM images of the Zn@Ni-P NWs obtained at different growth time. (a) 5 s, (b) 10 s, (c) 30 s, (d) 1min, (e) 5 min and (f) 15 min.

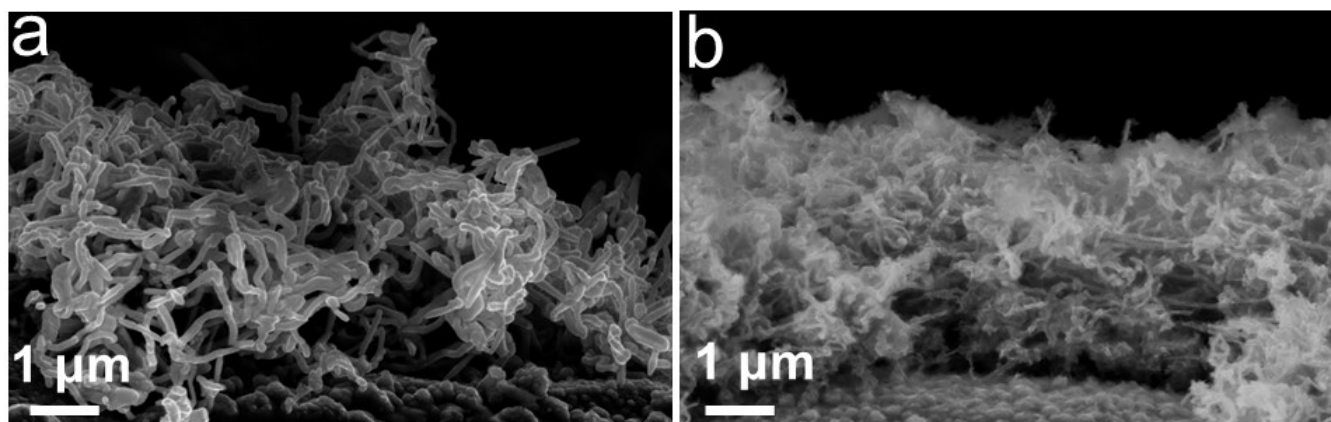


Figure S8. Cross-sectional SEM images of (a) Zn@Ni-P NWs, and (b) Ni-P/Ni(OH)₂ NTs.

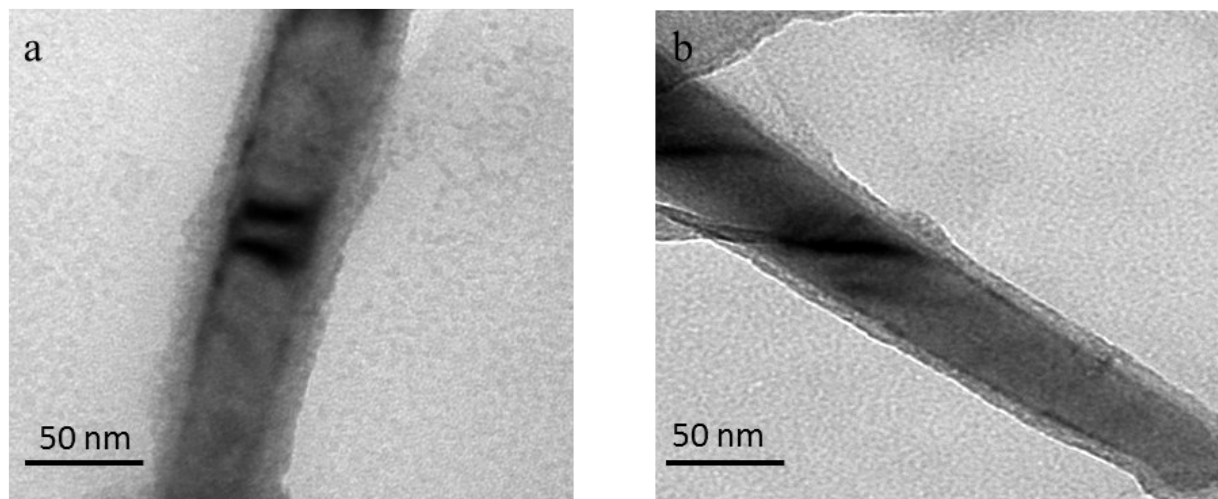


Figure S9. Zero-beam bright field TEM images showing a pair of twist contours. (a) and (b) are two different Zn@Ni-P NWs.

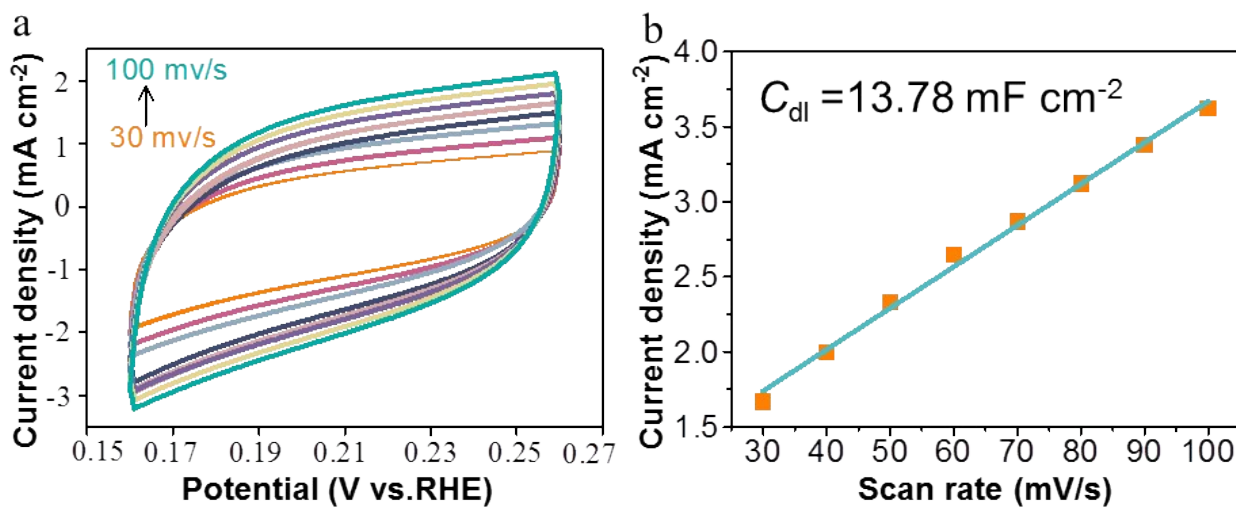


Figure S10. Electrochemical surface area (ECSA) measurements of the Ni-P/Ni(OH)₂ NTs in the 1 M KOH. (a) CV curves of the Ni-P/Ni(OH)₂ NTs with different scan rates in the non-faradic reaction range, (b) current differences plotted against scan rates. The linear slope is two times the double-layer capacitance C_{dl} .

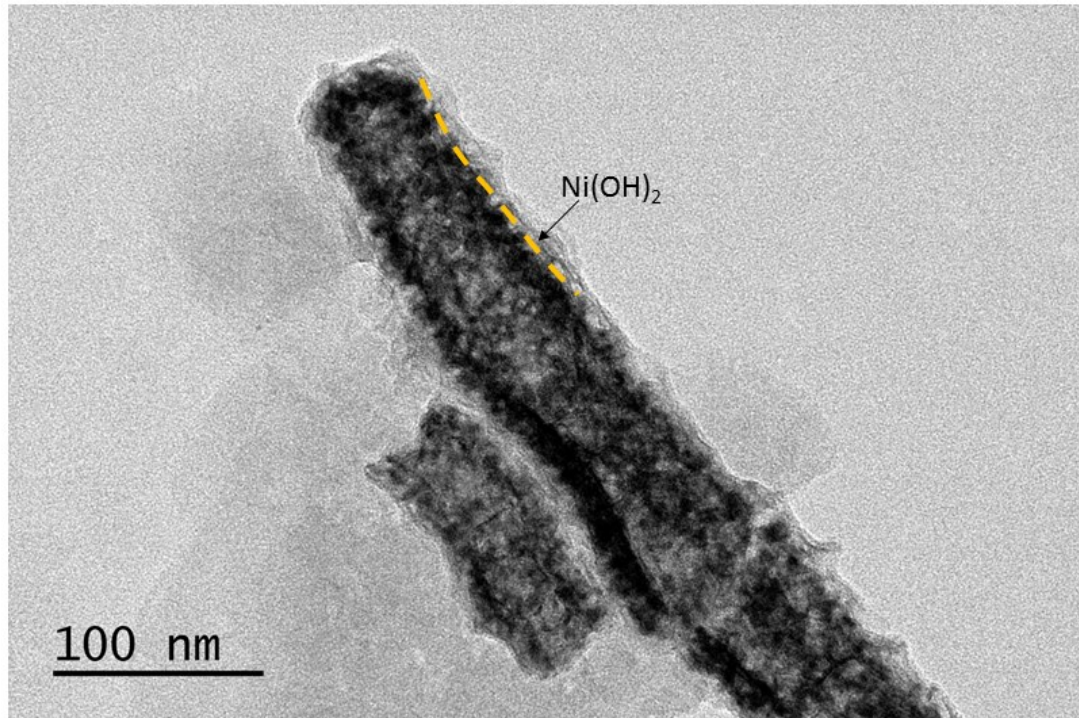


Figure S11. TEM image of the Ni-P/Ni(OH)₂ NTs.

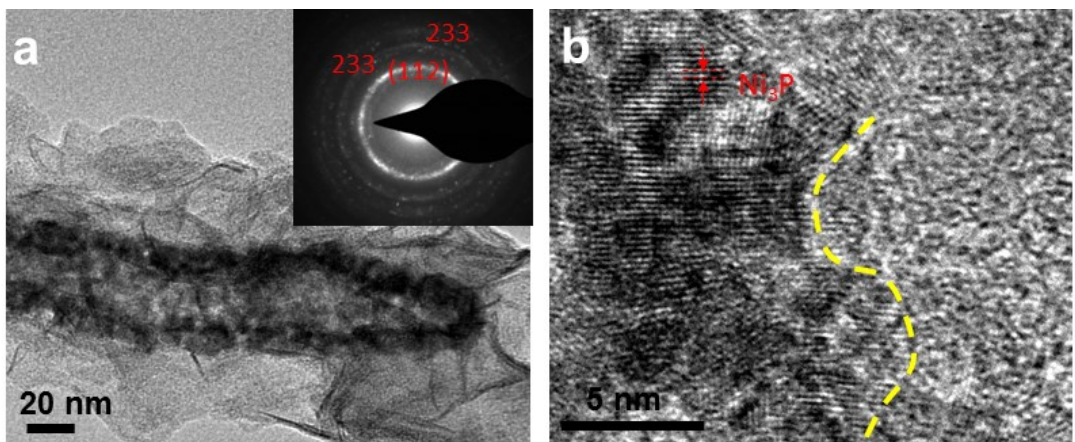


Figure S12. (a) TEM image of the crystalline/amorphous Ni-P/Ni(OH)₂ NTs . Insert is the SAED pattern; (b) HRTEM image of the crystalline/amorphous Ni-P/Ni(OH)₂ NTs.

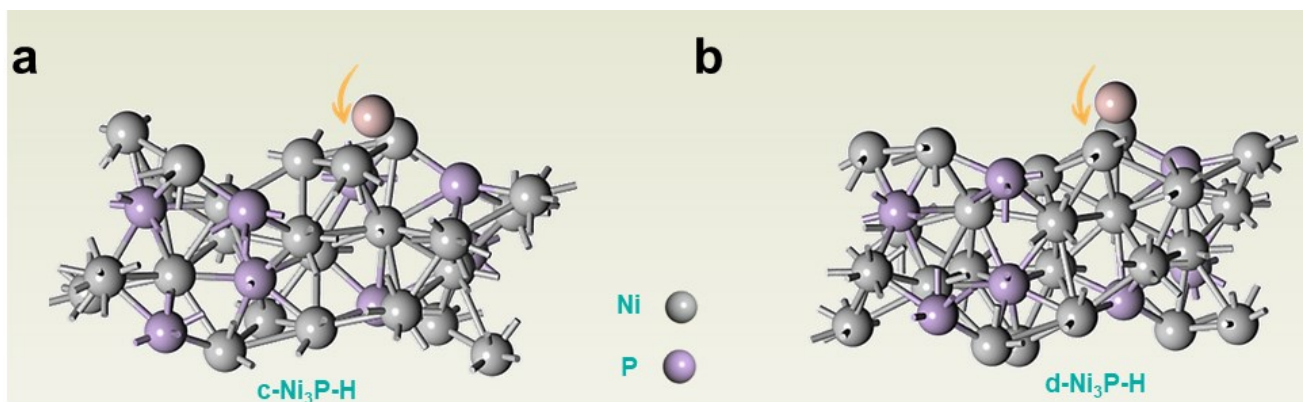


Figure S13. H* adsorption models of (a) c-Ni₃P, and (b) d-Ni₃P.

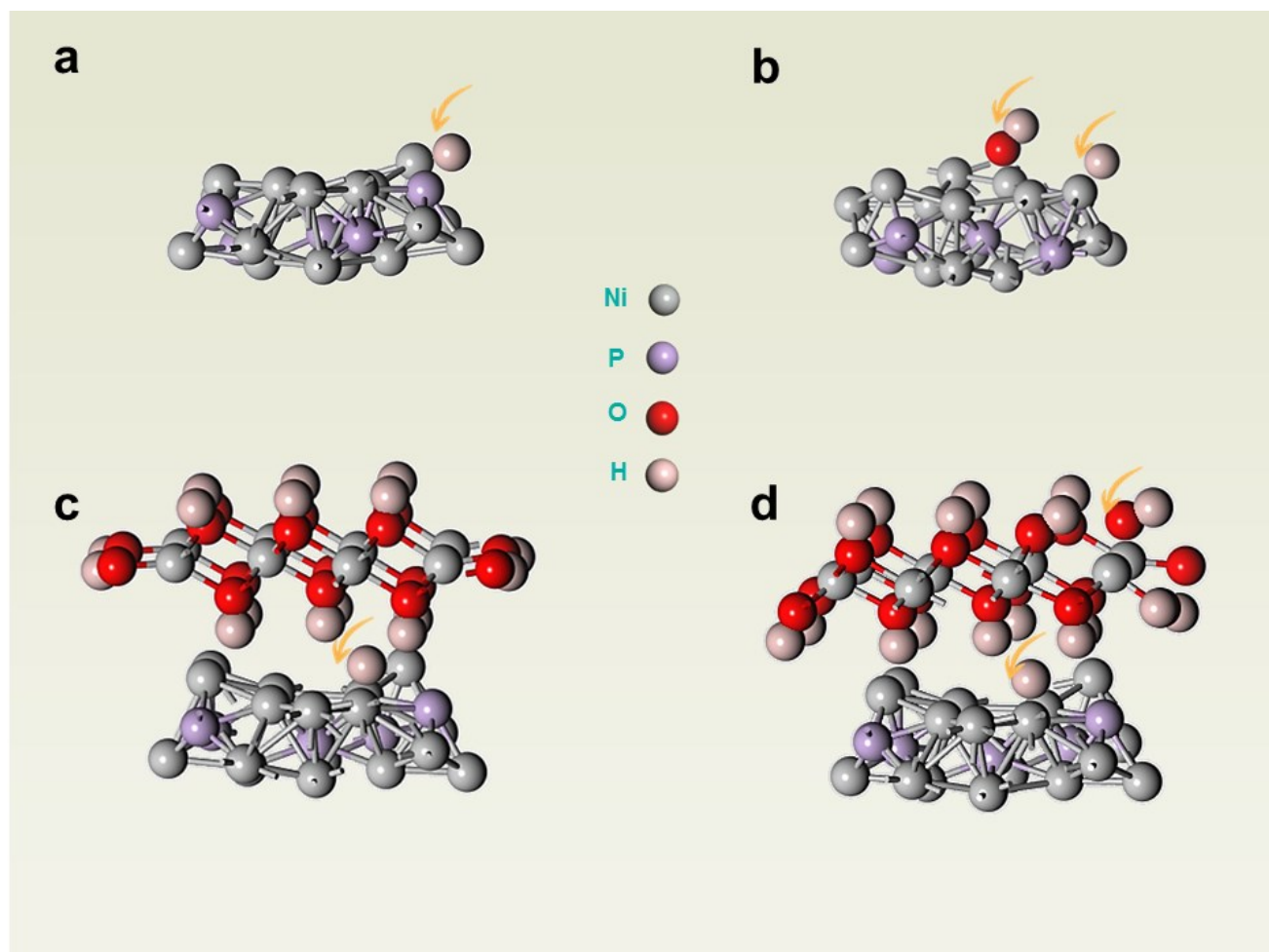


Figure S14. H* adsorption models of (a) amorphous Ni-P, and (c) heterostructure. OH-H* adsorption models of (b) amorphous Ni-P, and (d) heterostructure.

Table S1. Comparison of the overpotential of various transition metal phosphides in 1 M KOH at the current density of 10 mA cm⁻²

HER electrocatalysts	η_{10} (mV)	References
Ni ₅ P ₄	-47	1
This work	-54.7	
NiCoP _x NW	-58	2
MoP@RGO	-70	3
CoP/CNTs	-76	4
Mo-Ni ₂ P NW	-78	5
P-Mo ₂ C@NC	-83	6
MoP/CNTs	-86	7
Ni _{0.5} Co _{0.5} P	-87	8
CoP ₂ /RGO	-88	9
CO-P	-94	10
Mn-Ni ₂ P NS	-103	11
Cu ₃ P NS	-105	12
P-Co ₃ O ₄	-120	13
CoP ₃ NSs	-121	14
MoP/C	-125	15
Co ₂ P@NPC	-129	16
Cu ₃ P MSs	-130	17
Ni _{1.5} Fe _{0.5} P	-158	18
CoP/C	-163	19
Co/CoP-NC	-180	20

Table S2. Thermodynamic data used in the calculations of Gibbs free energy.

	E(eV)	Corrected value for G	G
H ₂ O	-14.218518	0.083711	-14.134807
H ₂	-6.77	-0.047005	-6.817005
c-Ni ₃ P	-183.32363	0	-183.32363
c-Ni ₃ P-H	-187.433554	0.164639 eV	-187.268915
d-Ni ₃ P	-175.46976	0	-175.46976
d-Ni ₃ P-H	179.45810	0.163664	-179.294436
Amorphous Ni ₃ P	-111.96887	0	-111.96887
Amorphous Ni ₃ P-H	-115.58735	0.204564	-115.382786
Amorphous Ni ₃ P-OH-H	-126.31185	0.504250	-125.8076
Heterstructure	-322.25478	0	-322.25478
Heterstructure-H	-325.74428	0.176825	-325.567455
Heterstructure-OH-H	337.00965	0.501006	337.510656

References

- 1 H. Wang, Y. Xie, H. Cao, Y. Li, L. Li, Z. Xu, X. Wang, N. Xiong and K. Pan, *ChemSusChem*, 2017, **10**, 4899-4908.
- 2 R. Zhang, X. Wang, S. Yu, T. Wen, X. Zhu, F. Yang, X. Sun, X. Wang and W. Hu, *Adv. Mater.*, 2017, **29**, 1605502.
- 3 G. Zhang, G. Wang, Y. Liu, H. Liu, J. Qu and J. Li, *J. Am. Chem. Soc.*, 2016, **138**, 14686-14693.
- 4 X. Zhang, S. Zhu, L. Xia, C. Si and F. Qu, *Chem. Commun.*, 2018, **54**, 1201-1204.
- 5 Y. Sun, L. Hang, Q. Shen, T. Zhang, H. Li, X. Zhang, X. Lyu and Y. Li, *Nanoscale*, 2017, **9**, 16674-16679.
- 6 Y. Gang, X. Feng, S. U. Khan, L. Xiao, W. Xi, H. Tan, Y. Ma, L. Zhang and Y. Li, *Chemistry – An Asian Journal*, 2018, **13**, 158-163.
- 7 X. Zhang, X. Yu, L. Zhang, F. Zhou, Y. Liang and R. Wang, *Adv. Funct. Mater.*, 2018, **28**, 1706523.
- 8 Y. Li, Z. Jiang, J. Huang, X. Zhang and J. Chen, *Electrochim. Acta*, 2017, **249**, 301-307.
- 9 J. Wang, W. Yang and J. Liu, *Journal of Materials Chemistry A*, 2016, **4**, 4686-4690.
- 10 N. Jiang, B. You, M. Sheng and Y. Sun, *Angew. Chem. Int. Ed.*, 2015, **54**, 6251-6254.
- 11 Y. Zhang, Y. Liu, M. Ma, X. Ren, Z. Liu, G. Du, A. M. Asiri and X. Sun, *Chem. Commun.*, 2017, **53**, 11048-11050.
- 12 A. Han, H. Zhang, R. Yuan, H. Ji and P. Du, *ACS Appl. Mater. Interfaces*, 2017, **9**, 2240-2248.
- 13 Z. Xiao, Y. Wang, Y. C. Huang, Z. Wei, C. L. Dong, J. Ma, S. Shen, Y. Li and S. Wang, *Energy & Environmental Science*, 2017, **10**, 2563-2569.
- 14 T. Wu, M. Pi, X. Wang, W. Guo, D. Zhang and S. Chen, *J. Alloys Compd.*, 2017, **729**, 203-209.
- 15 X. Liu, L. Zhang, M. Li and X. Hu, *Chem. Commun.*, 2018, **54**, 2502-2505.
- 16 C. Zhang, Z. Pu, I. Amiinu, Y. Zhao and J. Zhu, *Nanoscale Cambridge*, 2018, **10**, 2902-2907.
- 17 J. Hao, W. Yang, Z. Huang and C. Zhang, *Advanced Materials Interfaces*, 2016, **3**, 1600236.
- 18 H. Huang, C. Yu, C. Zhao, X. Han, J. Yang, Z. Liu, S. Li, M. Zhang and J. Qiu, *Nano Energy*, 2017, **34**, 472-480.
- 19 L. Yao, N. Zhang, Y. Wang, Y. Ni, D. Yan and C. Hu, *J. Power Sources*, 2018, **374**, 142-148.
- 20 Y. Hao, Y. Xu, W. Liu and X. Sun, *Materials Horizons*, 2018, **5**, 108-115.